Jurnal Kimia Valensi, Vol 9(1), May 2023, 30-41
Available online at Website: http://journal.uinjkt.ac.id/index.php/valensi

The Potential of Nanocellulose Acetate as Surfactant for Water-Vegetable Oil Systems

Ikhsan Ibrahim, Mia Ledyastuti*

Department of Chemistry, Bandung Institute of Technology
Ganesa street no.10, Bandung 40132, Indonesia

**Corresponding author: mia.ledyastuti@itb.ac.id*

Received: December 2022; Revision: March 2023; Accepted: May 2023; Available online: May 2023

Abstract

Indonesia, as an agricultural country, has a variety of abundant plants. Cellulose is a component in plants that can be modified to increase its economic value. Resizing cellulose to nanocellulose and modification of nanocellulose to nanocellulose acetate can increase its potential as a surfactant. Resizing cellulose can be done using the strong acid hydrolysis method. An acetic anhydride reagent was utilized to convert the surface hydroxyl functional group into acetyl. The successful production and modification of nanocellulose were confirmed using fourier transform infrared and particle size analysis characterization. The infrared absorption spectrum of cellulose and nanocellulose showed no difference in peaks. Particle size distribution showed that nanocellulose I (CNC I) and nanocellulose II (CNC II) has sizes of 142 nm and 319 nm, respectively. The property of nanocellulose molecules in an oil-water system was simulated using molecular dynamics with GROMACS 2020.6 software. Appropriate trends can be seen in the interfacial tension of water-vegetable oil systems. The value of interfacial tension decreases with the addition of nanocellulose acetate compared to the addition of nanocellulose. With the agreement between the experimental and computational results, nanocellulose acetate can act as a surfactant.

Keywords: Nanocellulose; computational method; surfactant

DOI: *10.15408/jkv.v9i1.29467*

1. INTRODUCTION

Indonesia is an agricultural country where most of the population works in agriculture, with the third most significant contribution to GDP (Gross Domestic Product) after the manufacturing and trade sectors (Kasdi, 2019). With the development of the agricultural industry, agricultural waste also increases. Most of this biomass waste is only used for animal feed and the rest is disposed of as organic waste, so the utilization of this waste is still relatively low in Indonesia (Waluyo, 2009). One of Indonesia's most massive biomass is cellulose, a polymer formed by a glucose monomer with a β(1→4) glycosidic bond. Due to the strong hydrogen bonds between glucose monomers (intramolecular) and between polymer chains (intermolecular), cellulose has fibrous, rigid, water-insoluble properties that can be found in plant cell walls, especially in stalks, stems, and all woody parts of the plant body (Nelson & Cox, 2008). The cellulose utilized in this research was isolated from empty palm oil fruit bunches (biomass waste) using the same extraction technique as earlier research by Sukmarani & Ledyastuti, (2019).

By changing the particle size to nanocellulose, new materials can be produced with different physical properties, such as viscosity, tensile strength, and surface-active properties (Shankaran, 2018). Nanocellulose (CNC) is a material derived from the physical or chemical treatment of cellulose that has a nano-size with a diameter of about 1-10 nm and a length of 10-100 nm (Lee et al., 2014). In its utilization as a surfactant, the hydroxyl groups of CNC need to be modified to disrupt the hydrogen bonds between glucose monomers. With this modification, the CNC surface is changed into a hydrophilic functional group, and the pyranose group is

P-ISSN: 2460-6065, E-ISSN: 2548-3013

hydrophobic, so it is predicted to reduce the value of the interfacial tension of water and vegetable oil. Acid hydrolysis with H_2SO_4 is one of the CNC synthesis techniques that can modify the surface chemical structure of CNC. Several things can affect the synthesized CNC: the type of acid, acid concentration, reaction time, and temperature during the hydrolysis treatment (Lee et al., 2014). In addition to hydrolyzing cellulose, H_2SO_4 can also modify CNC. H_2SO_4 can react with the hydroxyl group of CNC into anionic sulfate ester groups (OSO_3^-) (Klemm et al., 1998; Voronova et al., 2013).

Previous research on the synthesis of CNC used enzymatic, electrospinning, and acid hydrolysis techniques. According to Dewi et al., (2018) earlier research reported that the CNC produced by the electrospinning technique has a dimension of approximately 670 nm. The size of CNC produced by the enzymatic method is between 100 nm and 3,5 µm (Filson et al., 2009). Furthermore, 111 nm is the size of CNC made by the acid hydrolysis process (Wulandari et al., 2016). Based on these findings, acid hydrolysis is the best approach for synthesizing CNC because it requires only essential equipment and yields CNC of the correct size. H_2SO_4 and HCl are the typical acids employed in the acid hydrolysis process. The distinction is that H_2SO_4 hydrolysis creates sulfate esters (OSO_3^-), which make anionic repulsion and increase nanoparticle dispersion stability (Brinchi et al., 2013; Lee et al., 2014).

In this research, the surface modification was carried out by the acetylation method using acetic anhydride as a reagent. So later obtained nanocellulose acetate (O-CNC), which has hydrophilic acetyl, hydroxy, and hydrophobic pyranose ring group (Fallacara, Baldini, Manfredini, & Vertuani, 2018). O-CNC has the potential as a surfactant due to its amphiphilic structure. This causes the O-CNC to be at the interface of water and oil, reducing the interfacial tension (Bergfreund et al., 2021).

Computational and experimental methods were used in this study to determine the effectiveness of reducing the value of the water-oil interfacial tension by O-CNC, this method is a novelty from previous research. The computational method uses the GROMACS 2020.6 software to calculate the interfacial tension using the gmx_energy command. The experimental method uses the Du-Nouy tensiometer to determine the interfacial tension between water and vegetable oil.

2. MATERIALS AND METHODS

Materials

Cellulose (53.4% degree of crystallinity, Indonesia), H_2SO_4 (95-97% purity Merck, Germany), DMSO (Merck, Germany), pyridine (Merck, Germany), Na_2CO_3 (Merck, Germany), acetic anhydride (Merck, Germany), palm oil with organic, cosmetic, and food grade (Indonesia).

Instrumentation

The particle size of CNC was determined by Particle Size Analyzer (PSA) with Nano Particle Analyzer Horiba SZ-100. Infrared spectra of cellulose, CNC, and O-CNC were recorded on Bruker Alpha Fourier Transform Infrared Spectrometer (FTIR). The X-Ray diffraction (XRD) diffractograms were collected using Miniflex Rigaku Diffractometer. Fisher Scientific 20 Model 20 Surface Tensiometer measured water-vegetable oil systems interfacial tension (IFT).

Procedure

This research is divided into two, namely computational modeling and experimental. A computational method was carried out to obtain data on the value of the IFT produced by adding O-CNC compared to the addition of CNC. Wet lab experiments were carried out to synthesize CNC, modify CNC to obtain O-CNC, determine its properties as a surfactant, and other characterizations.

Nanocellulose Synthesis

The CNC synthesis step refers to the procedure carried out by Wulandari et al., (2016) with several modification steps (Wulandari et al., 2016). Pure cellulose is mixed with H_2SO_4 in a ratio (1:25). Variations in the concentration of H_2SO_4 and the hydrolysis time used were 50% (w/w) 7 minutes, and 45% (w/w) 7 minutes. After the reaction was complete, the mixture was stopped with distilled water ten times the volume of H_2SO_4 added. The suspension mixture obtained was centrifuged at 4500 rpm for 5 minutes. After that, the mixture was decanted to collect the residue for

ultrasonication. Sonication of the residue by adding 200 mL of aqua demineralization was carried out with an amplitude of 30 Hz for 5 minutes. The residue was then centrifuged for 8 cycles, in each cycle, the residue was washed with 200 mL aqua demineralization. In the last centrifugation cycle, the suspension was sonicated with 30 Hz amplitude for 5 minutes. After that, the CNC was placed in a vacuum oven at 40 °C for 3 hours to obtain a fine white powder.

Nanocellulose Modification

The modification research procedure used by Ning et al., (2020) was changed in several steps (Ning et al., 2020). In the first step, 10 mL of pyridine and 10 mL of acetic anhydride were mixed into 30 mL of anhydrous DMSO, which had been supplemented with 200 mg CNC. The suspension was stirred at room temperature (25 °C) for 2 hours. After the reaction, ice was added to the mixture, followed by centrifugation for 15 minutes. Sodium carbonate was added to remove acetic acid and neutralize the pH. The last step was cooling the mixture to get O-CNC as a precipitate.

Characterization

FTIR characterization was performed to analyze the cellulose, CNC, and O-CNC functional group. The difference in percent crystallinity between cellulose and CNC caused by various H_2SO_4 concentrations was calculated using XRD. Furthermore, PSA is used to measure the size of the CNC obtained from the acid hydrolysis method.

Determination of Surfactant Properties

The effectiveness of O-CNC as a surfactant was determined by measuring changes in interfacial tension (IFT) between a mixture of water and oil using the Du-Nouy ring method. This IFT measurement was carried out at various temperatures and concentrations of O-CNC. Using Radial Distribution Function (RDF) analysis and IFT calculations on dynamic trajectory results, surfactant characteristics can also be examined using molecular dynamics.

Molecular Dynamics

The simulation uses research procedures by Ledyastuti et al., (2021) and is modified in several steps (Ledyastuti et al., 2021). Molecular dynamics simulation of water and oil systems was carried out using GROMACS-2020.6. The command gmx insert-molecules multiplies water molecules in the liquid phase. Five thousand eight hundred thirty water molecules and 173 palmitic acid molecules were used for modeling the water and vegetable oil. Glucose dodecamer and acetylated glucose dodecamer were used as CNC and O-CNC. In the initial simulation, the CNC and O-CNC resided in the interphase position of water and vegetable oil. The simulation is carried out through the energy minimization stage. The NVT equilibration step adjusts the desired temperature. Then the NPT equilibration step adjusts the desired pressure, the production step, and the last is the analysis of production results. The analysis includes the trajectory visualization results, molecular density distribution analysis on the Z-axis, IFT analysis, and RDF analysis. All stages were carried out at 25, 30, 35, 40, 45, and 50 °C using a Nose-Hoover thermostat. Equilibration using NVT (number of molecules, constant volume, and temperature) was carried out for 125 ps, and NPT (number of molecules, constant pressure, and temperature) was carried out for 1000 ps. Simulations were carried out using a Parrinello-Rahman barostat to maintain a constant pressure at 1 bar according to a laboratory experiment measuring the IFT value (Parrinello & Rahman, 1998).

3. RESULTS AND DISCUSSION

The synthesis of CNC was carried out with an acid hydrolysis time of 7 minutes, and variations in the concentration of H_2SO_4 used were 45% (w/w) and 50% (w/w). The cellulose hydrolysis was carried out for 7 minutes to avoid burning the cellulose. The hydrolysis of cellulose was carried out at the 40 °C. The selection of a temperature of about 40 °C was based on the temperature commonly used in acid hydrolysis in previous research (Ningtyas et al., 2020; Wulandari et al., 2016; Xiong et al., 2012). FTIR, XRD, and PSA characterization reviewed the success of CNC synthesis. FTIR characterization examines whether there is a change in functional groups during the hydrolysis process. The mechanism of the hydrolysis reaction of cellulose with acids can be seen in **Figure 1**. The results of the FTIR spectrum can be seen in **Figure 2.** With CNC I, nanocellulose was obtained with

H_2SO_4 45% (w/w) and CNC II, nanocellulose was obtained with H_2SO_4 50% (w/w).

The absorption peak at 3300 cm^{-1} in the three spectra indicates the presence of O-H functional groups on the cellulose and CNC surface (Douglas et al., 2018). The peak at 2892 cm^{-1} indicates the presence of asymmetric stretching vibrations originating from the C-H group with sp^3 hybridization. In addition, the peak at 1316 cm^{-1} indicates the presence of C-O-C ether groups forming from β(1→4) glycosidic bonds in cellulose. The peak at 1060 cm^{-1} indicates the stretching vibration mode of the C-O-C group on the pyranose ring (Mandal & Chakrabarty, 2011). The absence of a peak at 1700 cm^{-1} means that the cellulose precursor is free from lignin (Dewi et al., 2017). It can also be noted that there is no difference in the absorption peaks for the absorption spectra of cellulose, CNC I, and CNC II. Therefore, acid treatment for the hydrolysis of cellulose does not alter the functional groups of cellulose (Wulandari et al., 2016).

The following characterization used XRD to calculate the degree of crystallinity and identify the type of cellulose utilized. The diffractogram for cellulose, CNC I, and CNC II can be seen in **Figure 3.**

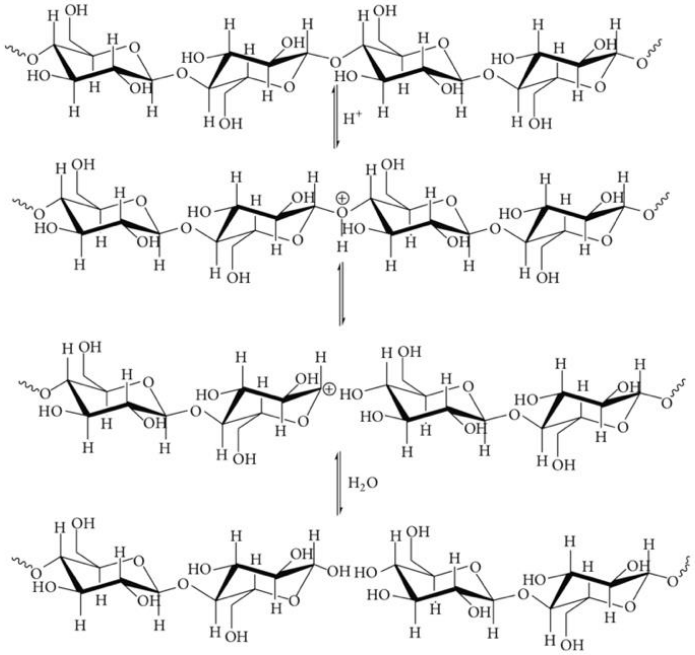

Figure 1. The reaction mechanism of cellulose acid hydrolysis (Lee et al., 2014)

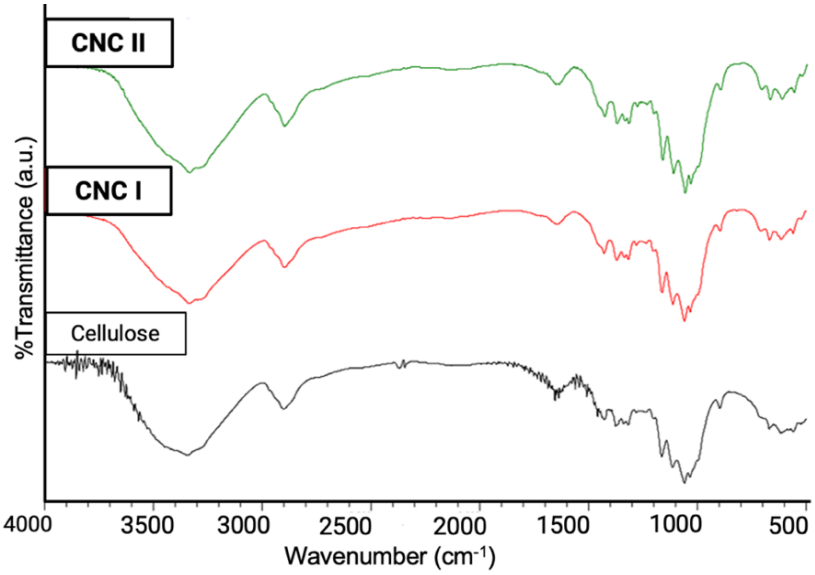

Figure 2. Cellulose, CNC I, and CNC II FTIR spectrum

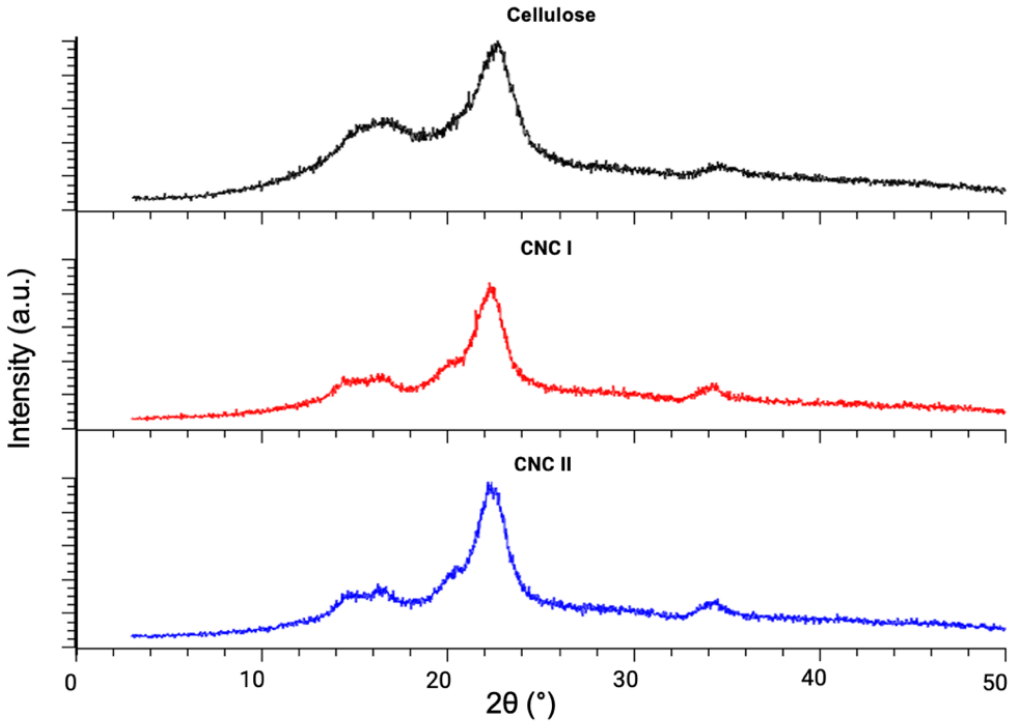

Figure 3. Cellulose, CNC I, and CNC II diffractogram

In the cellulose, CNC I, and CNC II diffractograms, a typical peak at 2θ of 14.5°, 16.5°, and 22.5° was observed, indicating that the type of cellulose used is a type I cellulose which has a parallel chain arrangement (French, 2014). Intensity contributors in the three prominent peaks have Miller indices (110), (110), and (200) (Gong et al., 2017). The degree of crystallinity can be calculated uisng equation (1).

$$C = \frac{I_{200} - I_{non-cr}}{I_{200}} \times 100\% \quad \text{.....(1)}$$

Where I_{200} is the intensity at 2θ 22.5° and Inon-cr is the intensity at 2θ of 18.5° (Terinte, Ibbett, & Schuster, 2017).

Percent crystallinity for cellulose, CNC I, and CNC II were 53.4%, 69.9%, and 71.1%, respectively. The increase in percent crystallinity in CNC II is affected by H_2SO_4 that plays a role in hydrolyzing the amorphous side of cellulose (because the amorphous side has a smaller density) (Lee et al., 2014; Wulandari et al., 2016). With the high concentration of H_2SO_4, the more hydrolyzed amorphous side so that the percentage of crystallinity is also higher.

The CNC I and CNC II particle size was measured by particle size analyzer (PSA). The particle size distribution of CNC I and CNC II can be seen in **Figure 4.** In the size distribution for CNC I, it can be seen that there are two dominant size distribution peaks. The first peak is at 142 nm and the second is at 7028 nm. CNC II also found two dominant size distribution peaks at 319 nm and 4364 nm. The size of the CNC is smaller with the concentration of H_2SO_4 is smaller. It indicates that the higher H_2SO_4 concentration does not result in a smaller CNC size (Wulandari et al., 2016). In addition, CNC with a higher concentration of H_2SO_4 produces a higher degree of crystallinity which causes long-range order, hence the particle size is larger for CNC II, and the size range for CNC II is smaller than CNC I (Alojaly & Benyounis, 2020). The CNC obtained with this hydrolysis method resulted in an appropriate smaller dimension of about 100 and 300 nm than the CNC obtained from the electrospinning method with the dimension of about 600 nm (Dewi et al., 2018).

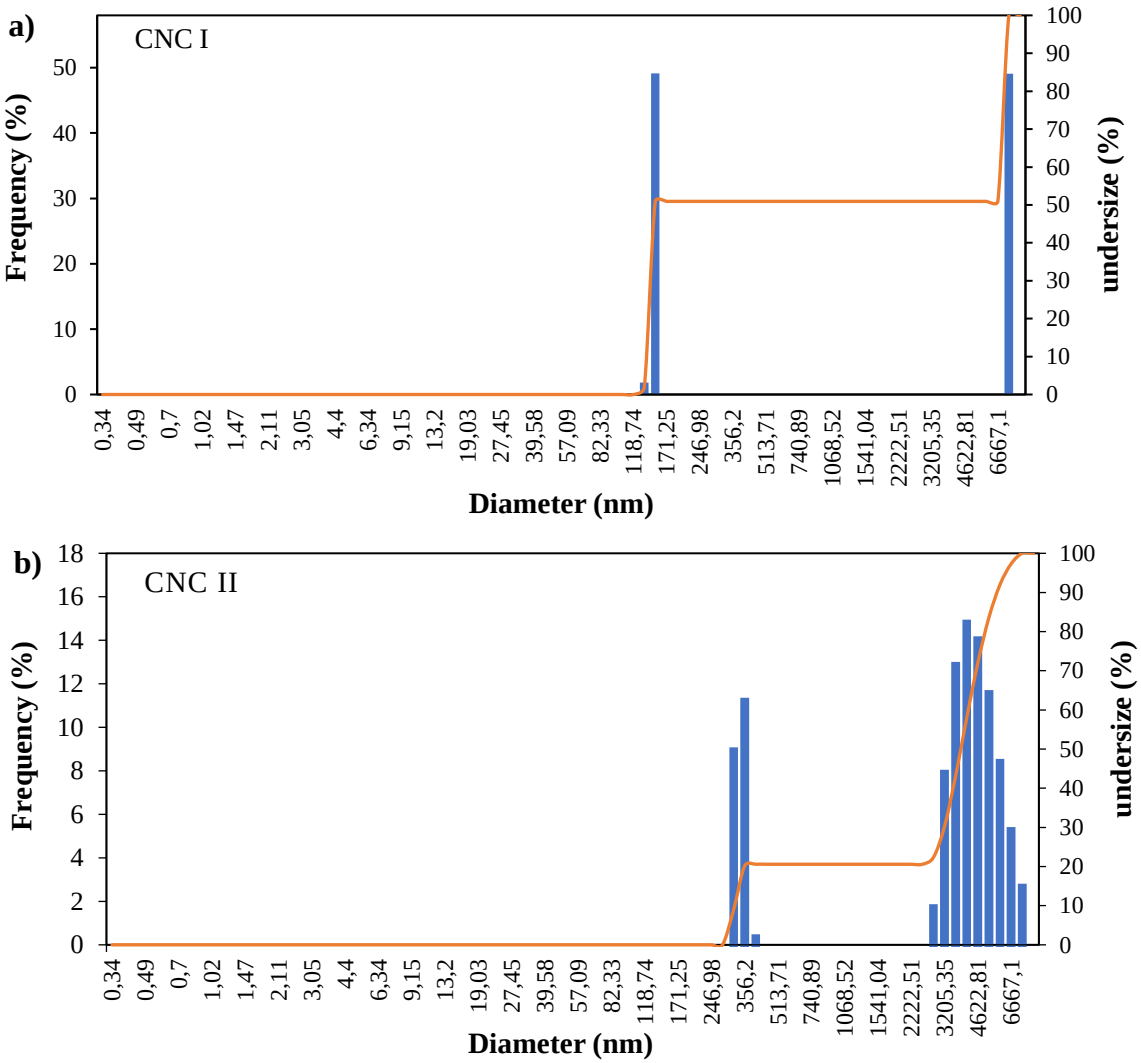

Figure 4. Particle size distribution (a) CNC I and (b) CNC II

Modification of Nanocellulose Into Nanocellulose Acetate

Modification of CNC was carried out by using pre-made CNC. The hydroxy functional group on the surface was modified using an acetic anhydride reagent which reacts with the hydroxy group on the CNC to form an acetyl group. The choice of acetic anhydride reagent was based on the good reactivity of acid anhydride compared to acetic acid. Acetic anhydride has an excellent leaving group (Klein, 2017). During the acetylation reaction, pyridine is added as a base catalyst, which plays a role in deprotonating the hydrogen in the alcohol with oxygen with an effective charge of +1 (Gero & Markham, 1951). A picture of the mechanism of the acetylation reaction is shown in **Figure 5.**

In analyzing the resulting functional groups, characterization was carried out using FTIR. The FTIR spectrum of CNC I and CNC II as comparison and O-CNC I, and O-CNC II as nanocellulose acetate can be seen in **Figure 6.** The broad peak at 3300 cm^{-1} on O-CNC I and O-CNC II indicates the presence of asymmetric vibrations in the O-H group. This shows the presence of unacetylated hydroxy groups. The presence of a new peak at 1750 cm^{-1} in the O-CNC I and O-CNC II absorption bands indicates the presence of a carbonyl group originating from the acetyl group. This confirmed that O-CNC was successfully formed (Deepashree et al., 2013). In addition, a new peak at 1250 cm^{-1} indicates the presence of a C-O-C functional group with a stretching vibration mode originating from the ester group (Krishni et al., 2013).

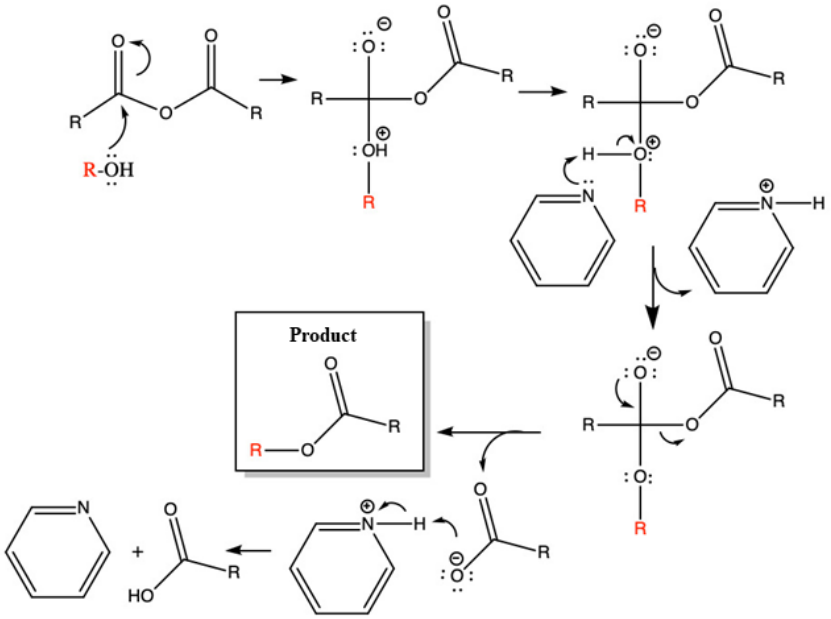

Figure 5. The mechanism of the acetylation reaction in CNC to O-CNC (Farmer & Clark, 2022)

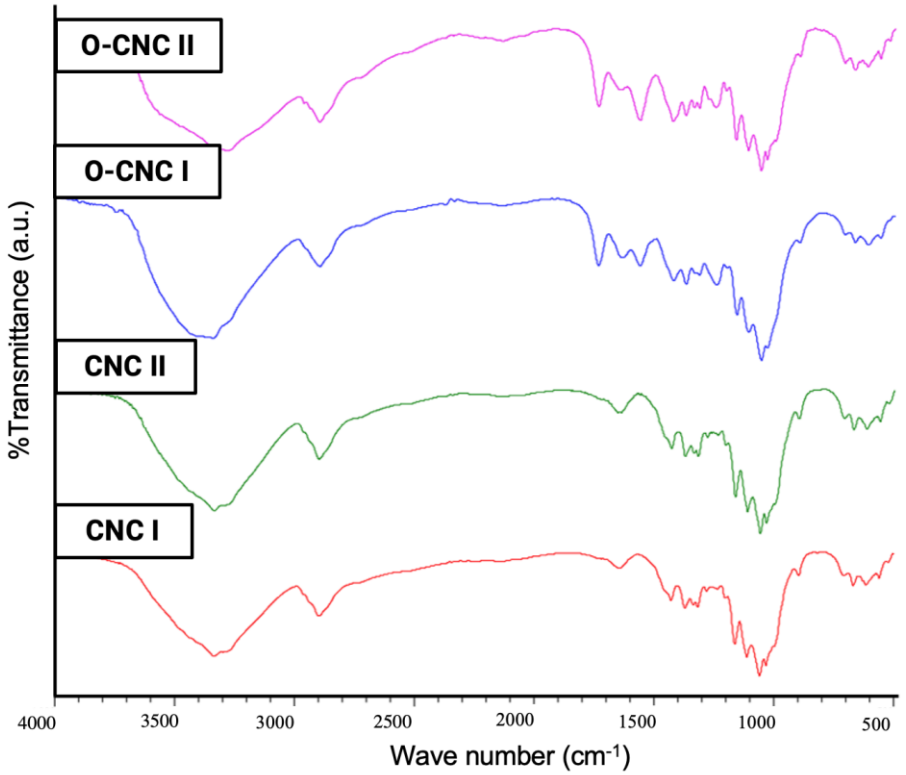

Figure 6. FTIR CNC I, CNC II, O-CNC I, and O-CNC II spectrum

The Potential of Nanocellulose Acetate as Surfactant

Surfactant is a type of material that can reduce the value of the IFT of the water and oil system because it can be adsorbed at the water and oil interface (Assadi et al., 2012). Therefore, the IFT value measurement for the water system with vegetable oil was carried out before and after the addition of CNC and O-CNC. The concentration used in testing the potential as a surfactant was carried out in the surfactant concentration range of 500 – 2000 ppm. The trend of the IFT value due to the addition of CNC I is shown in **Figure 7.** From this curve, it can be observed that the downward trend in IFT value is seen with the

increase in the concentration of CNC I. The decrease in IFT value is visible with the addition of 2000 ppm of CNC I.

Furthermore, measurements were made for the effect of adding CNC II. The trend of IFT value due to the addition of CNC II can be seen in **Figure 8.** From that curve, it can be observed that the downward trend in the IFT value appears in the early days of adding CNC II at a concentration of 500 – 1500 ppm. An increase in the IFT value was observed at a concentration of 2000 ppm, this IFT trend fracture may indicate the formation of micelles (already exceeding the CMC).

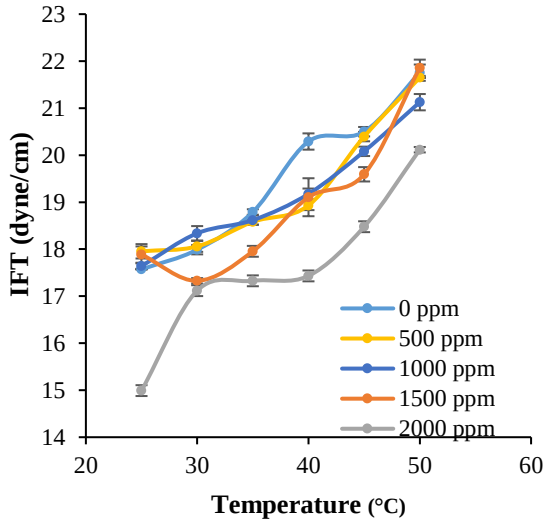

Figure 7. IFT trend of the water-palm oil system with added CNC I

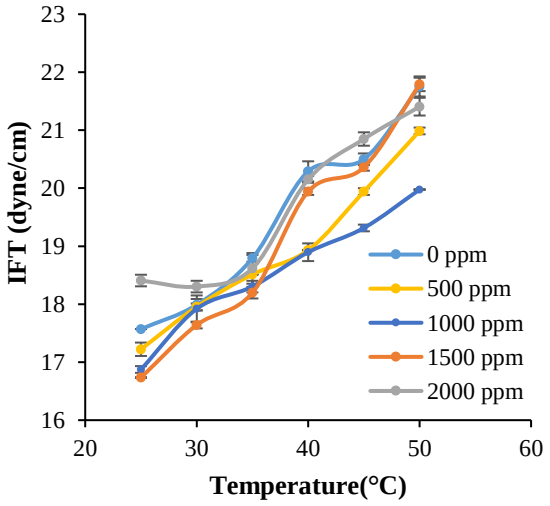

Figure 8. IFT trend of the water-palm oil system with added CNC II

The trend of IFT value due to the addition of O-CNC I can be seen in **Figure 9.** From **Figure 9,** the downward trend in IFT value appears with the gradual addition of O-CNC I. The decrease in the IFT trend, which is greater than the addition of CNC I, indicates O-CNC I can function as a better surfactant than CNC I.

The trend of IFT value due to the addition of O-CNC II can be seen in **Figure 10. Figure 10** observed that there was a match with the data on O-CNC I, where there was a decrease in the IFT value with increasing concentration of O-CNC II. In the O-CNC II concentrations of 1000 ppm, 1500 ppm, and 2000 ppm, no significant decrease in the IFT trend was observed. This result indicates the formation of micelles because the added surfactant has exceeded the CMC point (Moldes et al., 2020).

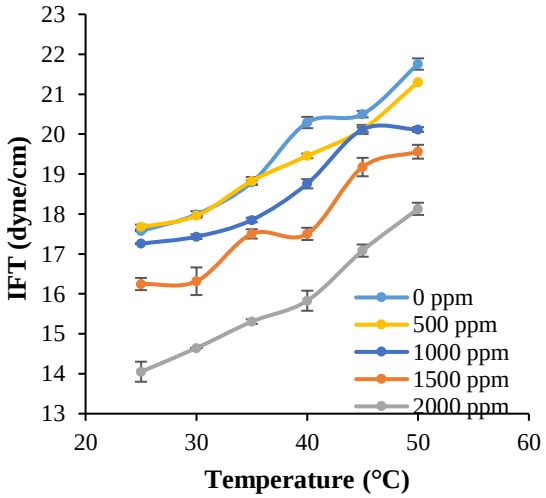

Figure 9. IFT trend of the water-palm oil system with **added** O-CNC I

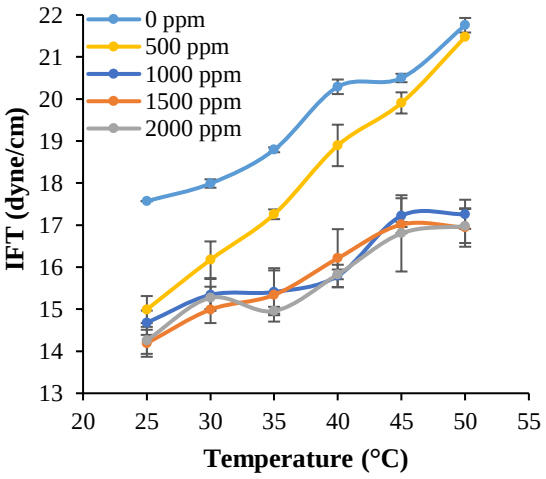

Figure 10. IFT trend of the water-palm oil system with added O-CNC I**I**

These results reveal that CNC does not reduce the IFT at the interface between water

and palm oil. This is consistent with earlier computational research. The IFT value produced by adding CNC without modification shows a higher IFT value (46.38 dyne/cm) than before adding CNC (43.63 dyne/cm) at room temperature in a water system with crude oil (Ledyastuti et al., 2021). The decrease in the IFT value can be seen from the addition of O-CNC to the water system with palmitic acid at room temperature from 43.63 dyne/cm to 40.21 dyne/cm. This shows that O-CNC can act as a better surfactant than CNC.

The productions result from molecular dynamics simulations were also analyzed to calculate the IFT value generated from each system. Initially, the simulation was carried out with three model systems: water-palmitic acid, water-(palmitic acid)-CNC, and water-(palmitic acid)-(O-CNC). The production stage was performed for 10 ns in these three systems with an NPT ensemble with temperature variations of 25, 30, 35, 40, 45, and 50°C. By calculating the IFT value computationally, it can be seen whether there is a match between the IFT trend generated and the IFT results measured in the experiment. The trend of changes in the value of the IFT from various temperatures for various model systems can be seen in **Figure 11.**

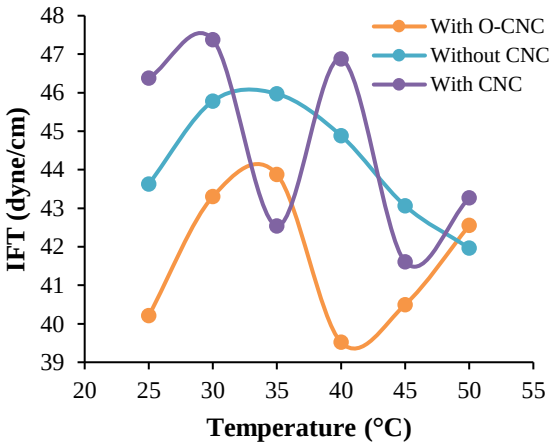

Figure 11. Trends in IFT values in various temperatures and various system variations

Furthermore, the production time was expanded for the water-palmitic acid, water-(palmitic acid)-CNC, and water-(palmitic acid)-(O-CNC) systems to 50 ns. The IFT trends generated from the three systems are shown in **Figure 12.**

From **Figure 12,** the correspondence between the experimental and computational results can be observed using IFT for the smallest value of O-CNC at each temperature. Furthermore, the analysis of what interactions occur in the O-CNC functional group is carried out. According to the definition, surfactants have polar and non-polar sides where the polar side interacts with the polar phase of the system, and the non-polar side interacts with the non-polar side of the system. This analysis can be done with the radial distribution function (RDF). The radial RDF describes the density variation around the reference atom as a function of the distance from a point (Sha et al., 2011). In this RDF, two analyses were carried out in which the carbonyl group acted as the polar side/group calculated the distance from the water, and the pyranose ring acted as the non-polar side calculated the distance from the palmitic acid.

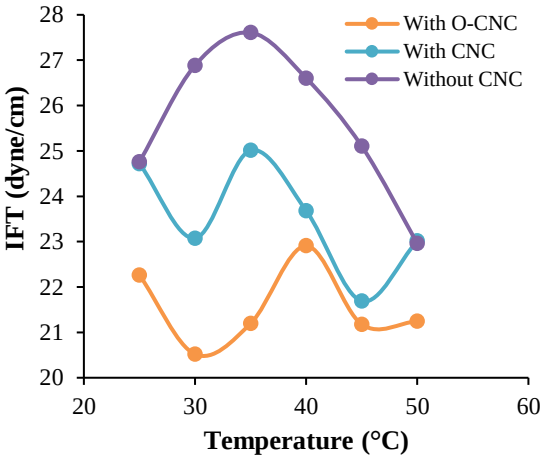

Figure 12. IFT results from 3 systems performed with a production time of 50 ns.

The RDF for the hydrophilic carbonyl side of O-CNC with respect to water is shown in **Figure 13.**

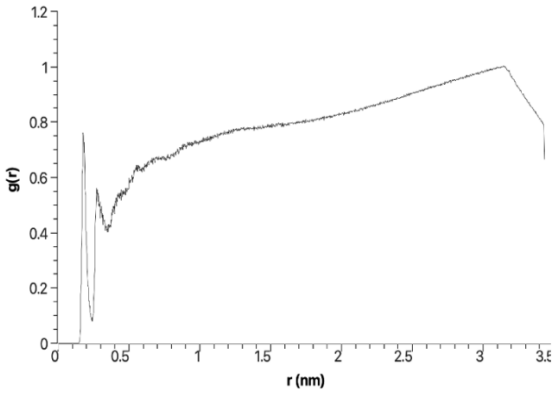

Figure 13. Radial distribution with carbonyl as reference and water as a particle whose distance is calculated (25°C temperature data, water-(palmitic acid)-(O-CNC) system)

In **Figure 13,** it is observed that there are sharp peaks at r of 0.18 and 0.27 nm. This result indicates that the carbonyl group in O-CNC interacts with water with hydrogen bond interaction because hydrogen bonds have a bond range between 0.12–0.3 nm (Grabowski, 2020).

Furthermore, the radial distribution for the hydrophobic side of the pyranose ring in O-CNC with respect to C in palmitic acid is shown in **Figure 14. Figure 14** shows sharp peaks for C1 and C2 in palmitic acid at r of 0.4–0.5 nm. This result indicates an interaction with van der Waals forces between C on the pyranose ring and C on the palmitic acid (Zhang, 2013). The results of this RDF support the explanation of the O-CNC that can reduce the IFT value in experimental measurements. The downward trend in the IFT value is due to the polar and non-polar groups in O-CNC interacting with both water and vegetable oil systems, so the IFT value decreases (Rosen, 2004).

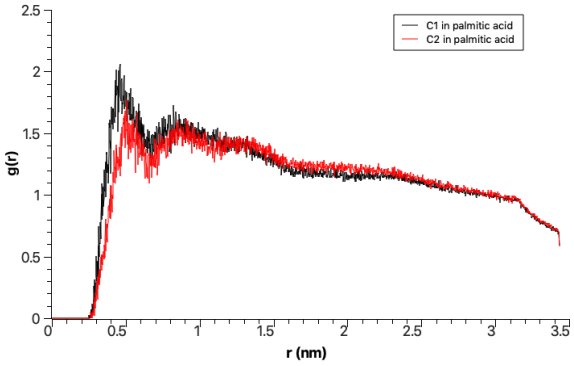

Figure 14. Radial distribution with C on the pyranose ring as a reference and palmitic acid as a particle whose distance is calculated (25°C temperature data, water-(palmitic acid)-(O-CNC) system)

4. CONCLUSION

CNC was successfully made by hydrolysis using H_2SO_4 to produce nanoparticle sizes for CNC I 142 nm and CNC II 319 nm. Furthermore, O-CNC was successfully synthesized from the previous CNC precursor using an acetic anhydride reagent. The FTIR spectrum showed that there are new peaks at 1721 cm^{-1} and 1250 cm^{-1}, which indicate the presence of C=O and C-O functional groups in O-CNC. In computational and experimental IFT measurement results, O-CNC reduces the IFT value in the water-vegetable oil system more than CNC. RDF analysis showed that the carbonyl group in O-CNC forms a hydrogen bond with water, while the C-C group on the pyranose ring interacts with C in palmitic acid by van der Waals forces. From the results of the analysis, it was found that O-CNC can act as a surfactant.

ACKNOWLEDGMENT

The authors would like to thank the ITB chemistry study program for providing laboratory facilities, including materials and tools. In addition, the authors thank the Theoretical Computation Chemistry-ITB research group for providing a “Renoir” server to carry out the Molecular Dynamics simulation process.

REFERENCES

Alojaly, H., Benyounis, K. Y. (2020). Packaging With Plastics and Polymeric Materials. *Reference Module in Materials Science and Materials Engineering*. https://doi.org/10.1016/B978-0-12-820352-1.00025-0

Assadi, Y., Farajzadeh, M. A., Bidari, A. (2012). Dispersive Liquid–Liquid Microextraction. *Comprehensive Sampling and Sample Preparation*, *2*, 181–212. https://doi.org/10.1016/B978-0-12-381373-2.00051-X

Bergfreund, J., Siegenthaler, S., Lutz-Bueno, V., Bertsch, P., Fischer, P. (2021). Surfactant Adsorption to Different Fluid Interfaces. *Langmuir*, *37*(22), 6722–6727. https://doi.org/10.1021/acs.langmuir.1c00668

Brinchi, L., Cotana, F., Fortunati, E., Kenny, J. M. (2013). Production of nanocrystalline cellulose from lignocellulosic biomass: Technology and applications. *Carbohydrate Polymers*, *94*(1), 154–169. https://doi.org/10.1016/j.carbpol.2013.01.033

Deepashree, C. L., Kumar, J., Prasad, A. G. D., Zarei, M., Gopal, S. (2013). FTIR spectroscopic studies on cleome gynandra – comparative analysis of functional group before and after extraction. *Romanian Journal of Biophysics*, *22*, 137–143.

Dewi, A. M. P., Edowai, D. N., Pranoto, Y., Darmadji, P. (2018). Sintesis nanoselulosa asetat dari ampas sagu dengan metode electrospinning. *Prosiding Seniar Nasional*

Sains dan Teknologi. 31–36. DOI: http://dx.doi.org/10.36499/psnst.v1i1.2358.

Dewi, A. M. P., Kusumaningrum, M. Y., Edowai, D. N., Pranoto, Y., Darmadji, P. (2017). *Ekstraksi Dan Karakterisasi Selulosa Dari Limbah Ampas Sagu*. *1*. Retrieved from https://garuda.ristekbrin.go.id/documents/detail/1151704

Douglas A. Skoog, F. James Holler, S. R. C. (2018). *Principles of Instrumental Analysis* (seven). United States of America. Retrieved from http://libgen.rs/book/index.php?md5=88BCED371633026E4266D23C9B1B3AF0

Fallacara, A., Baldini, E., Manfredini, S., Vertuani, S. (2018). Hyaluronic acid in the third millennium. *Polymers*, *10*(7). https://doi.org/10.3390/polym10070701

Filson, P. B., Dawson-Andoh, B. E., Schwegler-Berry, D. (2009). Enzymatic-mediated production of cellulose nanocrystals from recycled pulp. *Green Chemistry*, *11*(11), 1808–1814. https://doi.org/10.1039/b915746h

French, A. D. (2014). Idealized powder diffraction patterns for cellulose polymorphs. *Cellulose*, *21*(2), 885–896. https://doi.org/10.1007/S10570-013-0030-4

Gero, A., Markham, J. J. (1951). Studies on pyridines: I. The basicity of pyridine bases. *Journal of Organic Chemistry*, *16*(12), 1835–1838. https://doi.org/10.1021/JO50006A001/ASSET/JO50006A001.FP.PNG_V03

Gong, J., Li, J., Xu, J., Xiang, Z., Mo, L. (2017). Research on cellulose nanocrystals produced from cellulose sources with various polymorphs. *RSC Advances*, *7*(53), 33486–33493. https://doi.org/10.1039/c7ra06222b

Grabowski, S. J. (2020). *Understanding Hydrogen Bonds*. Royal Society of Chemistry. https://doi.org/10.1039/9781839160400

Waluyom, J. (2009). Pemanfaatan Limbah Biomassa sebagai Bahan Pembuatan Pakan Lembaga Ilmu Pengetahuan Indonesia. Retrieved January 11, 2022, from Prosiding Lokakarya Grassroot Innovation (GRI) BBPTTG-LIPI website: http://lipi.go.id/publikasi/pemanfaatan-limbah-biomassa-sebagai-bahan-pembuatan-pakan/10567

Kasdi. (2019). Pembangunan Perkebunan di Era Industri 4.0. Retrieved March 22, 2021, from https://www.pertanian.go.id/home/?show=news&act=view&id=4017

Klein, D. (2017). *Organic chemistry* (S. Bruno, Ed.). John Wiley & Sons, Inc.

Klemm, D., Philipp, B., Heinze, T., Heinze, U., & Wagenknecht, W. (1998). Comprehensive Cellulose Chemistry. In *Comprehensive Cellulose Chemistry*. Wiley. https://doi.org/10.1002/3527601929

Krishni, R., Foo, K. Y., Hameed, B. (2013). Adsorptive removal of methylene blue using the natural adsorbent-banana leaves. *Desalination and Water Treatment*, *52*, 6104–6112. https://doi.org/10.1080/19443994.2013.815687

Ledyastuti, M., Jason, J., Aditama, R. (2021). Effect of nanocellulose on water-oil interfacial tension. *Key Engineering Materials*, *874 KEM*, 13–19. https://doi.org/10.4028/www.scientific.net/KEM.874.13

Lee, H. V., Hamid, S. B. A., Zain, S. K. (2014). Conversion of Lignocellulosic Biomass to Nanocellulose: Structure and Chemical Process. *Scientific World Journal*, *2014*, 1–20. https://doi.org/10.1155/2014/631013

Mandal, A., Chakrabarty, D. (2011). Isolation of nanocellulose from waste sugarcane bagasse (SCB) and its characterization. *Carbohydrate Polymers*, *86*(3), 1291–1299. https://doi.org/10.1016/j.carbpol.2011.06.030

Moldes, A., Vecino, X., Rodríguez-López, L., Rincón-Fontán, M., Cruz, J. M. (2020). Biosurfactants: The use of biomolecules in cosmetics and detergents. *New and Future Developments in Microbial Biotechnology and Bioengineering: Microbial Biomolecules: Properties, Relevance, and Their Translational Applications*, 163–185. https://doi.org/10.1016/B978-0-444-64301-8.00008-1

Nelson, D. L., Cox, M. M. (2008). *Principles Of Biochemistry* (5th ed.). New York: Sara Tenney.

Ning, L., You, C., Zhang, Y., Li, X., Wang, F. (2020). Synthesis and biological evaluation of surface-modified nanocellulose hydrogel

loaded with paclitaxel. *Life Sciences*, *241*, 117137. https://doi.org/10.1016/j.lfs.2019.117137

Ningtyas, K. R., Muslihudin, M., Sari, I. N. (2020). Sintesis nanoselulosa dari limbah hasil pertanian dengan menggunakan variasi konsentrasi asam synthesis of nanoselulosa from agricultural waste using variation acid concentration. *Jurnal Penelitian Pertanian Terapan*, *20*(2), 142–147.

Parrinello, M., Rahman, A. (1998). Polymorphic transitions in single crystals: A new molecular dynamics method. *Journal of Applied Physics*, *52*(12), 7182. https://doi.org/10.1063/1.328693

Rosen, M. J. (2004). *Surfactants And Interfacial Phenomena*. New Jersey.: John Wiley & Sons, Inc.

Sha, W., Wu, X., Keong, K. G. (2011). Molecular dynamics (MD) simulation of the diamond pyramid structure in electroless copper deposits. *Electroless Copper and Nickel–Phosphorus Plating*, 82–103. https://doi.org/10.1533/9780857090966.1.82

Shankaran, D. R. (2018). Chapter 14 - Cellulose Nanocrystals for Health Care Applications. In S. Mohan Bhagyaraj, O. S. Oluwafemi, N. Kalarikkal, & S. Thomas (Eds.), *Applications of Nanomaterials* (pp. 415–459). Woodhead Publishing. https://doi.org/https://doi.org/10.1016/B978-0-08-101971-9.00015-6

Farmer, S., Clark, J. (2022). *Map: Organic Chemistry (Smith)*.

Sukmarani, G., Ledyastuti, M. (2019). The Properties of Microcellulose as Enhanced Oil Recovery Agent. *Journal of Physics: Conference Series*, *1245*(1). https://doi.org/10.1088/1742-6596/1245/1/012041

Terinte, N., Ibbett, R., Schuster, K. C. (2017). *Overview on native cellulose and microcrystalline cellulose I structure studied by X-ray diffraction (WAXD): Comparison between measurement techniques Overview On Native Cellulose And Microcrystalline Cellulose I Structure Studied By X-Ray Diffraction*. (January 2011).

Voronova, M. I., Surov, O. V., Zakharov, A. G. (2013). Nanocrystalline cellulose with various contents of sulfate groups. *Carbohydrate Polymers*, *98*(1), 465–469. https://doi.org/10.1016/j.carbpol.2013.06.004

Wulandari, W. T., Rochliadi, A., Arcana, I. M. (2016). Nanocellulose prepared by acid hydrolysis of isolated cellulose from sugarcane bagasse. *IOP Conference Series: Materials Science and Engineering*, *107*(1). https://doi.org/10.1088/1757-899X/107/1/012045

Xiong, R., Zhang, X., Tian, D., Zhou, Z., Lu, C. (2012). Comparing microcrystalline with spherical nanocrystalline cellulose from waste cotton fabrics. *Cellulose*, *19*. https://doi.org/10.1007/s10570-012-9730-4

Zhang, X.-J. (2013). Van der Waals Forces. *Encyclopedia of Tribology*, 3945–3947. https://doi.org/10.1007/978-0-387-92897-5_457